JGR Atmospheres

RESEARCH ARTICLE
10.1029/2018JD029918

A Multiscale Analysis of the Tropospheric and Stratospheric Mechanisms Leading to the March 2016 Extreme Surface Ozone Event in Mexico City

Bradford S. Barrett[1], Graciela B. Raga[2], Armando Retama[3,4], and Christopher Leonard[1]

[1]Oceanograhpy Department, U.S. Naval Academy, Annapolis, Maryland, USA, [2]Centro de Ciencias de la Atmósfera, Universidad Nacional Autónoma de Mexico, Mexico City, Mexico, [3]Secretaría del Medio Ambiente del Distrito Federal, Dirección de Monitoreo Atmosférico, Mexico City, Mexico, [4]Independent Scholar, Mexico City, Mexico

Key Points:
- High surface ozone concentrations occur in the days immediately following an extreme cutoff low pressure system
- Cutoff low pressure system connected to variability of the Pacific jet stream
- High ozone concentrations caused by troposphere-stratosphere exchange (at first) then by local generation accelerated by strong UV radiation

Correspondence to:
B. S. Barrett,
bbarrett@usna.edu

Citation:
Barrett, B. S., Raga, G. B., Retama, A., & Leonard, C. (2019). A multiscale analysis of the tropospheric and stratospheric mechanisms leading to the March 2016 extreme surface ozone event in Mexico City. *Journal of Geophysical Research: Atmospheres*, *124*. https://doi.org/10.1029/2018JD029918

Received 31 OCT 2018
Accepted 26 MAR 2019
Accepted article online 2 APR 2019

Abstract This study analyzed the physical mechanisms behind a multiday high surface ozone (O_3) event in Mexico City in March 2016. In early March, a strong zonal jet stream over the Pacific Ocean amplified and underwent wave breaking. An unusual cutoff low pressure system then migrated across central Mexico, with 200-hPa geopotential heights among the lowest in the reanalysis historical record (1948 to present). A tropopause fold on the west side of the cutoff low transported O_3-rich air from the stratosphere into the troposphere and resulted in high O_3 concentrations all the way to the surface. The stratospheric intrusion began on 09 March and ended on 12 March, but surface O_3 concentrations continued to rise, peaking on 14 March. Given the deep boundary layer observed on 12 March, it is very likely that remnants of the stratospheric O_3 in the midtroposphere at the regional level could have been entrained into the boundary layer. Furthermore, our analysis indicates that as the cutoff low progressed eastward, the pronounced low-level thermal inversion and reduced ventilation observed on subsequent days (13–15 March) contributed to elevated concentrations of O_3 precursors, which together with strong UV radiation, led to efficient photochemical production of O_3 and to the very large values observed in several of the monitoring stations (up to 210 parts per billion on 14 March). Finally, mitigation measures put into place by authorities reduced both the number of vehicles on the road and the resulting nighttime titration, possibly extending the duration of dangerous O_3 levels in the city.

1. Introduction

Tropospheric ozone (O_3) is a major secondary air pollutant affecting human health (Anenberg et al., 2009; Levy et al., 2005; Mena-Carrasco et al., 2009; Riojas-Rodríguez et al., 2014; Yan et al., 2013; Yang et al., 2014). Ground level O_3 is primarily produced during photochemical reactions between organic precursors (volatile organic compounds, VOCs, and methane CH_4), CO, and nitrogen oxides (NO and NO_2; abbreviated NO_x hereafter) in the presence of UV radiation (Monks et al., 2015; Simpson et al., 2014). A complex coupling of primary emissions, dynamic transport, and chemical transformations all lead to the generation of surface O_3 (Jacob, 1999; Wang et al., 2017). Regions with poor ventilation, strong UV radiation, and large urban boundary layers (with plentiful anthropogenic precursors) are prone to experience O_3 concentrations in excess of 400 parts per billion (ppb; EPA, 2006).

In addition to diurnal photochemical generation, tropospheric O_3 can also originate in the stratosphere, transported downward via a process known as stratosphere-troposphere exchange (STE). For many decades, STE has been known to play an important role in the chemical composition of the troposphere, as it brings O_3-rich stratospheric air into the troposphere (Crutzen, 1973; Danielsen, 1968; Levy, 1972). A primary mechanism for STE is the tropopause fold (Akritidis et al., 2016; Cooper et al., 2004, 2010; Holton et al., 1995; Reiter, 1975; Staley, 1960), and indeed, up to 70% of the subtropical STE mass flux in winter can be attributed to tropopause folds (Sprenger et al., 2003). Deep stratospheric intrusions have also been implicated in springtime exceedances of surface O_3 limits, including in Colorado (Langford et al., 2009), Nevada (Langford et al., 2015, 2017), California (Langford et al., 2012), and Arizona and New Mexico (Lin et al., 2012). Intrusions of stratospheric air into the troposphere occur globally and are most common in winter and spring, when midlatitude and cutoff low activity is at its peak (Holton et al., 1995; Kentarchos

& Davies, 1998; Nieto et al., 2005). Both the photochemical production of surface O_3 in Mexico City and the role of planetary-scale, synoptic-scale, and mesoscale weather systems have been studied extensively (as reviewed below). However, cutoff lows, tropopause folds, and STE events, to our knowledge, have not yet been examined for their potential role in surface O_3 variability in Mexico City, a gap that this study helps to fill.

Air pollution in Mexico City has been the subject of intense study since the 1960s, as summarized by Raga et al. (2001). More recently, intensive field campaigns (e.g., Edgerton et al., 1999; Molina et al., 2007; Molina et al., 2010) have provided ample measurements documenting that conditions in Mexico City differ from other urbanized regions in the world due to emission rates, VOC speciation, ambient temperatures, and its altitude (affecting photolysis rates), resulting in the general high level of pollution. Modeling and measurement studies in Mexico City indicate that O_3 formation over the core region of the city is generally VOC sensitive, while the surrounding region is limited either by VOCs or NO_x depending on the meteorological conditions (Lei et al., 2008; Molina et al., 2010; Song et al., 2010). This VOC-limited regime is supported by radical budget studies showing chain termination by NO_x chemistry (Wood et al., 2009; Volkamer et al., 2010, Sheeny et al., 2010), and by the weekend effect described by Stephens et al. (2008). The problem of surface O_3 is exacerbated because Mexico City, a megacity with 21 million inhabitants, receives intense solar radiation at its tropical latitude (19.4°N) and high elevation (more than 2,200 m above sea level; Lei et al., 2008). The city is also in a shallow basin, effectively preventing ventilation of polluted air (de Foy et al., 2006; Edgerton et al., 1999; Fast & Zhong, 1998; García-Yee et al., 2018; Whiteman et al., 2000).

During the cold dry season (December–February), the warm dry season (March–May), and the warm wet season (June–August) months, clear skies in the morning yield strong insolation that promotes the rapid generation of surface O_3 via photochemical conversions of anthropogenic precursor emissions near the surface. Cloud cover throughout the day in the cool wet season (September–November) generally reduces insolation and thus reduces overall O_3 concentrations. Past studies, including both short-duration intensive field campaigns (Raga & Le Moyne, 1996) and long-term climatologies (Barrett & Raga, 2016; Rodríguez et al., 2016), have noted a primary relationship between O_3 concentration and UV radiation. In those studies, days with more UV radiation were associated with elevated surface O_3 concentrations. Afternoon O_3 concentrations in winter, spring, and summer are somewhat modulated by dilution due to the development of a deep and fairly well-mixed atmospheric boundary layer (ABL), which can grow to heights up to 3,000 m above ground level in the afternoon due to strong convective overturning (Doran et al., 1998; Raga et al., 1999; Zelaya-Angel et al., 2010). However, that reduction in O_3 concentrations presumes that the deepening of the ABL results in mixing between contaminated surface-layer air and more pristine air higher up. If the air directly above the ABL has higher O_3 concentrations, including those introduced into the troposphere by an STE event, then a deepening ABL will access that reservoir of high O_3 and transport some of it to the surface, acting to increase surface O_3 via net downward O_3 flux (Dempsey, 2014; Monks et al., 2015; Ott et al., 2016; Škerlak et al., 2014).

While there is a general agreement on the physical mechanisms associated with surface O_3 production, there are still uncertainties. Therefore, it is often difficult to develop effective control strategies for reducing ambient O_3, and even after decades of efforts, extreme surface O_3 events do occur that are not anticipated. This study was motivated by one such event in March 2016. In that event, surface O_3 concentrations reached hazardous levels for several consecutive days. What made that event unusual, and what led us to examine the physical atmospheric and chemical processes responsible in more detail, was that it was immediately preceded in time by the passage of an intense and unusual upper tropospheric trough. In this study, potential physical and policy mechanisms responsible for the high O_3 event are explored. The remainder of this article is organized as follows: the data sets analyzed and methods used for analysis are presented in section 2. The results of the study are presented in section 3. Finally, the results are discussed in section 4.

2. Data and Methods

Hourly surface concentrations of O_3 (in ppb) during the month of March 2016 were analyzed across the Mexico City metropolitan area using measurements at 23 observing stations that are part of the *Red Automática de Monitoreo Atmosférico* network (Figure 1 and Table 1) managed by the local government.

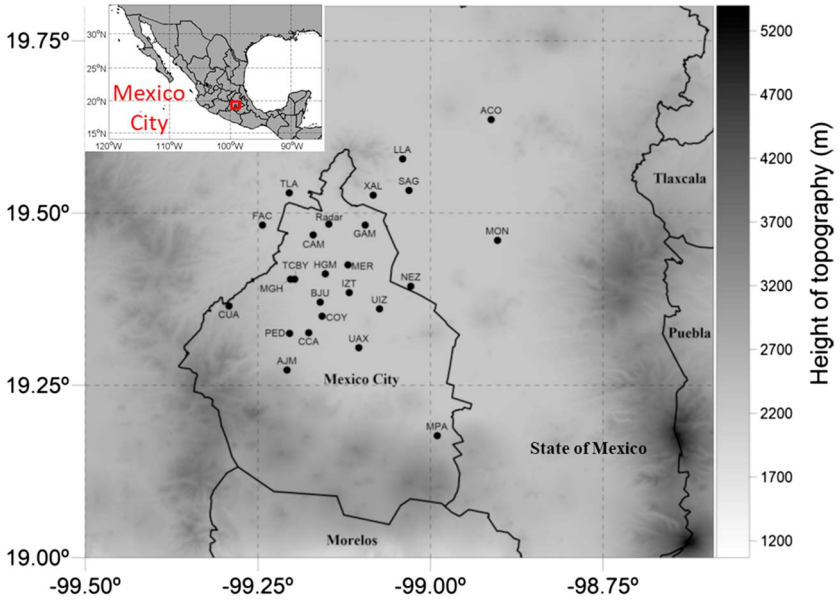

Figure 1. Locations of the 23 air quality observing locations in Mexico City. Station abbreviations listed in Table 1. Upper air observing site location is indicated as TCBY, and radar wind profiler indicated as Radar. Shading indicates elevation above sea level (in m), and political boundaries showing Mexico City and surrounding states are in black curves with labels.

Table 1
List of Observing Stations Used in This Study and Latitude (°N), Longitude (°W), Elevation Above Sea Level (in m), and Variable Measured

Three-Letter Code	Station	Latitude	Longitude	Elevation (m Above Sea Level)	Variables: Ozone (O_3), Carbon Monoxide (CO), UV-B Radiation (UVB)
ACO	Acolman	19.6	−98.9	2198	O_3, CO
AJM	Ajusco Medio	19.3	−99.2	2619	O_3, CO
BJU	Benito Juárez	19.4	−99.2	2250	O_3, CO
CAM	Camarones	19.5	−99.2	2233	O_3, CO
CCA	Centro de Ciencias de la Atmósfera	19.3	−99.2	2280	O_3, CO
COY	Coyoacán	19.4	−99.2	2260	O_3
CUA	Cuajimalpa	19.4	−99.3	2704	O_3, CO
FAC	FES Acatlán	19.5	−99.2	2299	O_3, CO
GAM	Gustavo A. Madero	19.5	−99.1	2227	O_3
HGM	Hospital General de México	19.4	−99.2	2234	O_3, CO
IZT	Iztacalco	19.4	−99.1	2238	O_3, CO
LLA	Los Laureles	19.6	−99.0	2230	O_3
MER	Merced	19.4	−99.1	2245	O_3, CO, UVB
MGH	Miguel Hidalgo	19.4	−99.2	2366	O_3, CO
MON	Montecillo	19.5	−98.9	2252	O_3, CO
MPA	Milpa Alta	19.2	−99.0	2594	O_3, CO
NEZ	Nezahualcóyotl	19.4	−99.0	2235	O_3, CO
PED	Pedregal	19.3	−99.2	2326	O_3, CO
SAG	San Agustín	19.5	−99.0	2241	O_3, CO, UVB
TLA	Tlalnepantla	19.5	−99.2	2311	O_3, CO, UVB
UAX	UAM Xochimilco	19.3	−99.1	2246	O_3, CO
UIZ	UAM Itzapalpa	19.4	−99.1	2221	O_3, CO
XAL	Xalostoc	19.5	−99.1	2160	O_3, CO

Hourly surface concentrations of CO (in parts per million (ppm)) from 20 observing stations were also analyzed (Table 1). Hourly UV-B (in units of minimal erythema dose (MED)/hr) was analyzed at the three stations that reported UV-B in March 2016 (Table 1), and daily UV-B averages at those stations were computed by averaging all UV-B measurements during daylight hours on each day. Vertical profiles of horizontal wind velocity (taken at 6-min time intervals and about 60-m vertical spacing) were obtained from a vertical wind profiler (915-MHz DeTec Raptor VAD-BL radar wind profiler) located in Mexico City (19.48°N, 99.15°W; elevation 2,255 m above sea level; "Radar"; Figure 1) from 09–17 March 2016. Additionally, vertical profiles of temperature, dew point temperature, and horizontal winds were examined from radiosonde observations from the Tacubaya Observatory in Mexico City (station TCBY 76679; 19.4°N, 99.2°W; elevation 2,313 m above sea level; Figure 1) at 1200 UTC from 05 to 17 March 2016 and an additional 0000 UTC sounding on 12 March 2016.

On the large scale, meteorological and chemical (when available) information from three widely used atmospheric reanalyses—National Centers for Environmental Prediction (NCEP)/National Center for Atmospheric Research (NCAR) reanalysis (Kalnay et al., 1996), ERA-Interim reanalysis (Dee et al., 2011), and MERRA-2 reanalysis (Gelaro et al., 2017)—were analyzed. Upper troposphere winds and geopotential heights at 200 hPa were analyzed at 6-hr intervals during March 2016 using observations from the NCEP/NCAR reanalysis (Kalnay et al., 1996) at a horizontal grid spacing of 2.5° latitude by 2.5° longitude. That reanalysis was selected because it extends back to 1948, thus allowing the determination of the climatological frequency of occurrence of upper tropospheric troughs and the unusualness of the event of interest. Six-hourly height anomalies at 200 hPa were calculated for March 2016 by subtracting the daily long-term (1948–2017) mean for March from each 6-hr value (uncertainty with the historical observations in the early part of that record motivated the choice to use daily averages instead of 6-hr averages). Zonal eddy kinetic energy (EKE) for March 2016 was calculated at each grid point in the reanalysis as $\mathrm{EKE} = 0.5(u-\overline{u})^2$, where u is the 6-hr zonal wind observation and $\overline{u}$ the long-term (March 1948–2017) mean daily zonal wind (Rieck et al., 2015). Daily zonal EKE was also calculated for each day in March, 1948–2017, via the same method. To quantify the behavior of zonal EKE in the subtropical Pacific jet stream, anomalies were averaged over a rectangular region extending from 20° to 40°N and 140° to 120°W. The rectangular region was chosen to correspond to the subtropical Pacific Ocean west of Mexico. Anomalies were weighted by the cosine of their latitude to account for the gradual decrease in grid area with increasing latitude. To evaluate the intensity of the upper level closed low that crossed Mexico and the southern United States, 200-hPa heights were averaged in a small rectangular region centered over central Mexico extending from 17.5°N–22.5°N to 105°–95°W.

Finally, to evaluate the behavior of the STE, variables from two other atmospheric reanalyses were examined. The ERA-Interim and MERRA-2 reanalyses were selected for O_3 analysis because they have sophisticated diagnostics not available in the NCEP/NCAR reanalysis. Results from both ERA-Interim and MERRA-2 are shown to allow comparison between the two products. First, potential vorticity (PV in potential vorticity units, PVU; 1 PVU is 10^{-6} m^2 s^{-1} K kg^{-1}) and O_3 concentrations (in ppb) from the ERA-Interim reanalysis (Dee et al., 2011) were analyzed at 6-hr intervals during March 2016 on a horizontal grid of 0.75° latitude by 0.75° longitude and centered on the grid point (19.5°N, 99.0°W) closest to Mexico City. Second, PV and O_3 concentration (in ppb) from the NASA MERRA-2 reanalysis (Gelaro et al., 2017; GMAO, 2015) were analyzed at 3-hr intervals during March 2016 on a horizontal grid of 0.5° latitude by 0.625° longitude, and also centered on the grid point (19.0°N, 99.375°W) closest to Mexico City. While each reanalysis has some limitations in handling O_3 in the troposphere (Dragani, 2011; Trickl et al., 2014), and tropopause folds tend to be better captured in data sets with horizontal spacing of less than 50 km (Büker et al., 2005; Lin et al., 2012; Ott et al., 2016), both reanalysis products have been used to successfully analyze STE in previous studies (Knowland et al., 2017; Škerlak et al., 2015).

3. Results

3.1. Surface O_3 Event

In the afternoon of 12 March 2016, air quality monitoring stations in the Mexico City metropolitan region area measured hourly surface O_3 concentrations as high as 163 ppb and 8-hr average concentrations as high as of 112 ppb (Tables 2 and 3 and Figure 2a). Of the 23 stations in the government-run Red Automática de

Table 2
Daily Maximum 1-hr O_3 Concentrations (in ppb), From 9 to 16 March 2016

Station/Day	9	10	11	12	13	14	15	16	17	18	19	20
ACO	36	61	62	**113**	**102**	**117**	**114**	**112**	**119**	64	48	57
AJM	45	65	66	**112**	**163**	**146**	**122**	**140**	**109**	72	55	76
BJU	41	62	60	**151**	**167**	**183**	**140**	**127**	**116**	68	50	83
CAM	35	63	62	**148**	**157**	**160**	**141**	**130**	**118**	77	46	59
CCA	41	62	60	**124**	**164**	**150**	**127**	**137**	**111**	67	55	78
COY	41	63	63	**134**	**157**	**166**	**129**	**125**	**112**	65	53	78
CUA	49	67	69	**149**	**181**	**210**	**148**	**151**	**122**	59	48	82
FAC	39	56	69	**158**	**137**	**185**	**156**	**143**	**83**	73	18	61
GAM	37	62	64	**163**	**157**	**161**	**145**	**135**	**138**	79	47	77
HGM	37	61	57	**153**	**170**	**189**	**148**	**135**	**120**	70	48	77
IZT	39	57	58	**147**	-	-	-	**120**	**122**	61	49	77
LLA	31	57	58	**142**	**109**	**137**	**133**	**112**	**116**	-	-	-
MER	34	47	53	**128**	**136**	**144**	**120**	**112**	**102**	62	36	63
MGH	37	63	60	**141**	**165**	**190**	**142**	**132**	**110**	71	46	74
MON	34	57	55	**131**	**108**	**108**	**97**	87	**101**	48	41	49
MPA	-	-	-	76	**118**	**102**	87	82	88	59	57	63
NEZ	-	54	57	**129**	**132**	**112**	**119**	**105**	**113**	57	49	58
PED	39	67	66	**129**	**171**	**165**	-	-	-	-	-	-
SAG	31	55	56	**145**	**106**	**124**	**107**	**96**	**127**	66	50	58
TLA	37	60	61	**111**	**102**	**144**	**143**	**120**	**113**	42	41	47
UAX	39	58	59	**98**	**128**	**112**	**128**	**113**	**110**	63	57	68
UIZ	35	52	56	**115**	**124**	**109**	**116**	**99**	**101**	57	48	59
XAL	23	43	41	87	78	87	77	67	81	49	33	44

Note. Values exceeding 95 ppb (which trigger mitigation controls) are noted in bold. Missing data are indicated with hyphen.

Table 3
Daily Maximum 8-hr O_3 Concentrations (in ppb), From 9 to 16 March 2016

Station/Day	9	10	11	12	13	14	15	16	17	18	19	20
ACO	33	58	61	90	88	**104**	50	50	56	40	43	45
AJM	42	63	63	93	**139**	**119**	69	74	60	47	46	56
BJU	31	56	57	**104**	**123**	**131**	45	46	41	34	45	55
CAM	27	56	57	**103**	**115**	**113**	42	40	39	28	40	43
CCA	32	56	57	95	**129**	**118**	47	49	47	29	46	54
COY	34	57	61	**100**	**121**	**123**	46	48	47	33	47	54
CUA	40	62	64	**110**	**136**	**152**	71	60	57	41	40	61
FAC	30	54	60	**112**	**108**	**128**	55	52	-	34	-	47
GAM	31	58	61	**112**	**120**	**119**	46	46	49	31	42	58
HGM	28	56	55	**108**	**124**	**131**	46	44	49	31	41	51
IZT	30	53	55	**101**	-	-	-	39	45	27	42	52
LLA	27	53	56	99	89	**111**	44	41	43	-	-	-
MER	-	45	-	89	**100**	**103**	35	33	37	24	32	42
MGH	28	57	56	**104**	**123**	**133**	47	44	43	28	38	50
MON	30	53	51	86	87	88	44	39	43	35	35	42
MPA	-	-	-	69	94	97	69	66	60	53	48	47
NEZ	-	50	54	88	95	94	42	40	45	33	39	43
PED	35	61	61	97	**133**	**128**	-	-	-	-	-	-
SAG	26	52	52	**101**	92	**102**	40	38	42	30	40	41
TLA	29	55	-	87	86	**108**	43	40	41	20	36	36
UAX	34	55	58	85	**113**	**102**	55	52	50	42	45	51
UIZ	28	49	54	87	95	92	44	-	-	34	39	43
XAL	19	36	40	65	63	67	28	25	29	20	28	34

Note. Values exceeding 100 ppb are noted in bold. Missing data are indicated with hyphen.

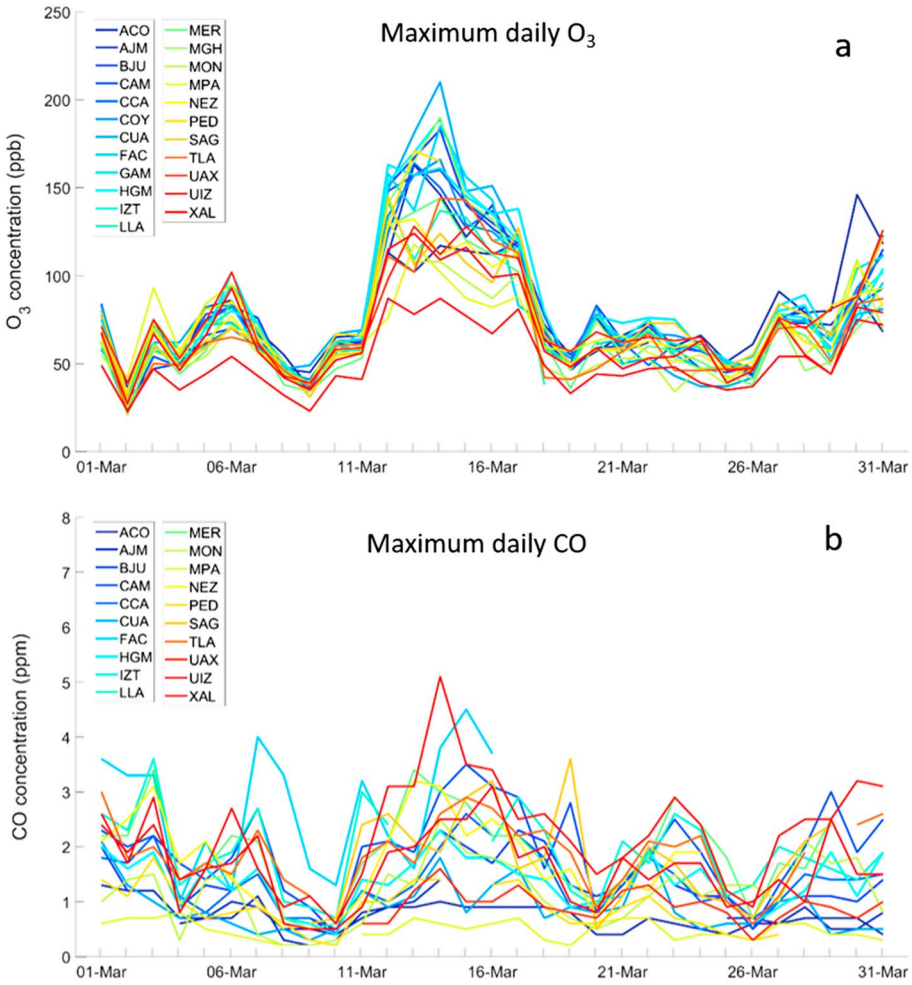

Figure 2. (a) Maximum hourly surface O_3 concentrations (in ppb) and (b) maximum hourly surface CO concentrations each day, 01–31 March 2016, at stations in the RAMA observing network across the Mexico City metropolitan area. Station locations provided in Figure 1 and abbreviations in Table 1. 5–6, 12–13, 19–20, and 26–27 March are weekend days.

Monitoreo Atmosférico network in operation in March 2016, all but two exceeded the Mexican national standard (hourly concentrations of 95 ppb), and all exceeded the Mexican standard for 8-hr mean of 70 ppb and the World Health Organization 8-hr guideline of 70 ppb (World Health Organization, 2006). Maximum daily CO concentrations also began to increase on 11 March 2016 (Figure 2b). Surface O_3 concentrations worsened on 13 March 2016, reaching a maximum peak hourly concentration of 171 ppb at one station and concentrations above 150 ppb at six other stations (Table 2). Eight-hour concentrations peaked at 139 ppb and all but one exceeded the World Health Organization guideline (Table 3). Surface CO concentrations also increased on 13 March 2016, exceeding 3 ppm at several stations (Figure 2b), although CO concentrations at other stations remained low (less than 1 ppm) throughout the event. Despite returning to low baseline O_3 concentrations (<5 ppb) during the night hours due to NO_x titration (not shown), O_3 conditions continued to deteriorate on 14 March 2016, reaching a peak of 210 ppb at one station, exceeding 150 ppb at eight others, and exceeding the Mexican hourly and 8-hr standards at 22 of the 23 reporting stations across the metropolitan region (Tables 2 and 3). The outlier station, Xalostoc (XAL), is located in the northeast in one of the most polluted regions of the metropolitan region, characterized by high levels of primary pollutants that are carried by the dominant winds toward the south-southwest of Mexico City. The strong emission of fresh nitrogen oxides near XAL contributes to the rapid depletion of ozone by titration. Concentrations continued at elevated levels for the next three days, with afternoon measurements not returning below the Mexican hourly standard until 18 March 2016

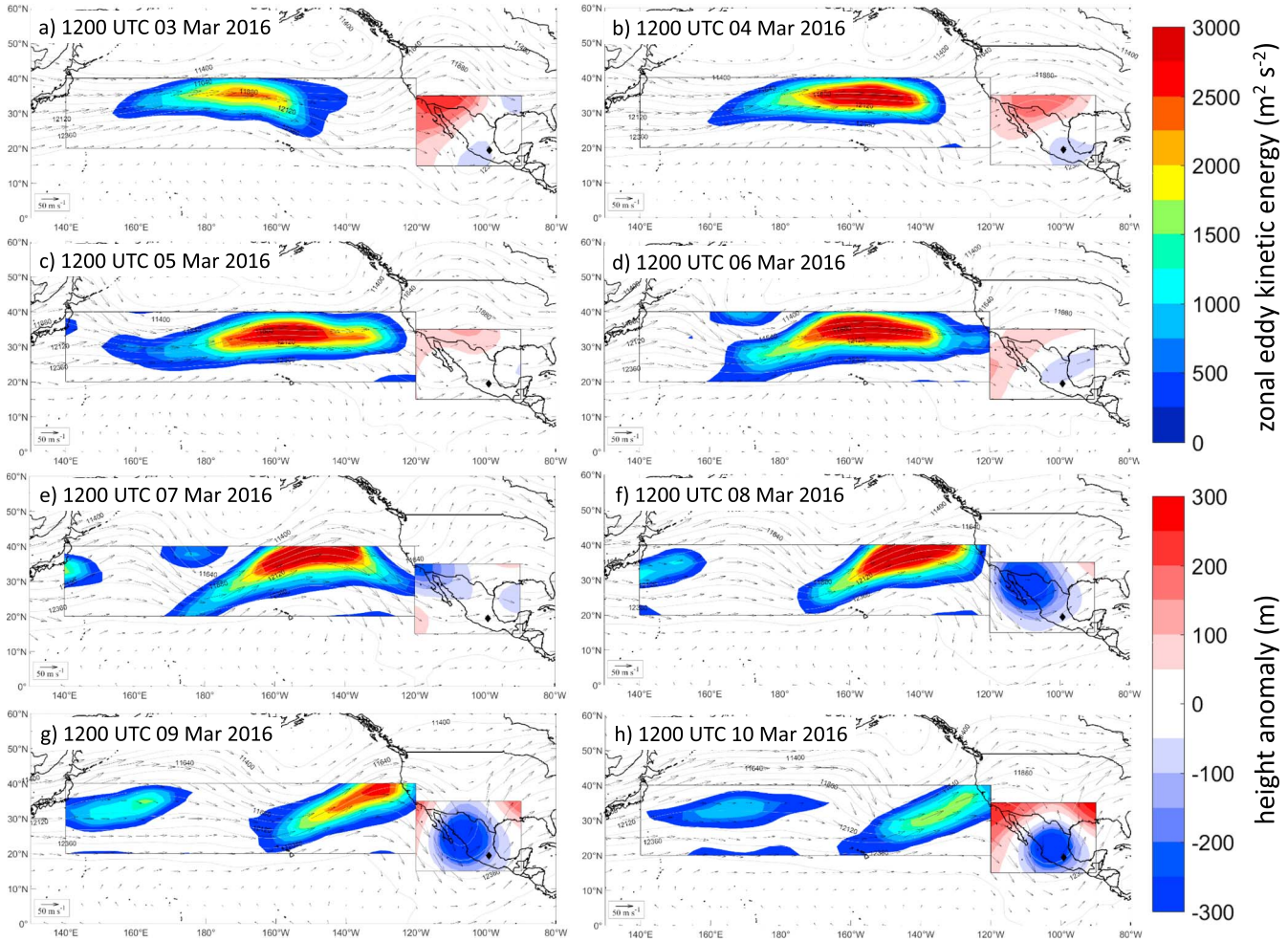

Figure 3. Winds (in m/s), zonal eddy kinetic energy per unit mass (in m^2/s^2), and geopotential height anomalies (in m) at 200 hPa for (a–h) 1200 UTC 3–10 March 2016. All data were from NCEP/NCAR reanalysis. Zonal EKE is only shown for 140°–120°W, 20°–40°N, and those values are used for the analyses in Figures 4 and 5. Height anomalies are only shown for 105°–95°W, 17.5°–22.5°N, and those values are used for the analyses in Figures 6 and 7.

(Tables 2 and 3). Concentrations of CO also remained high throughout the O_3 event, returning to less than 2 ppm on 19 March 2016 (Figure 2b).

3.2. Evolution of the Upper Tropospheric Trough

At 1200 UTC on 03 March 2016, seven days before the lowest 200-hPa height in central Mexico and nine days before the onset of dangerous surface O_3 conditions, upper tropospheric flow across the subtropical Pacific from 20° to 40°N exhibited a slightly wavy pattern, with a ridge axis along 180°E, a trough axis along 145°W, another ridge axis along 120°W, and a positively tilted trough axis across central Mexico (Figure 3a). Zonal EKE at 1200 UTC 03 March 2016 was at the lowest value (near 250 m^2/s^2) of the first 10 days of March (Figure 4a) and was very close to the long-term mean (a standard anomaly of only +0.3; Figure 4b). However, from 04 to 05 March, 200-hPa flow over the subtropical Pacific strengthened considerably (Figures 3b and 3c), and by 1200 UTC 05 March 2016, a distinct wind maximum was evident north of Hawaii along 35°N (Figure 3c). This jet maximum was associated with nearly zonal flow, reflected in strongly positive zonal EKE (over 450 m^2/s^2) in the same region (Figure 4a).

By 1200 UTC 06 March 2016, troughing was evident around 170°E, but the jet, and its associated zonal EKE maximum, stretched across a broad region of the subtropical Pacific, from the base of the trough at 170°E eastward to 120°W and from 25° to 40°N (Figure 3d). On this date, the mean zonal EKE over the jet region reached near 600 m^2/s^2, which was more than 4 standard deviations above normal (Figure 4). Daily mean

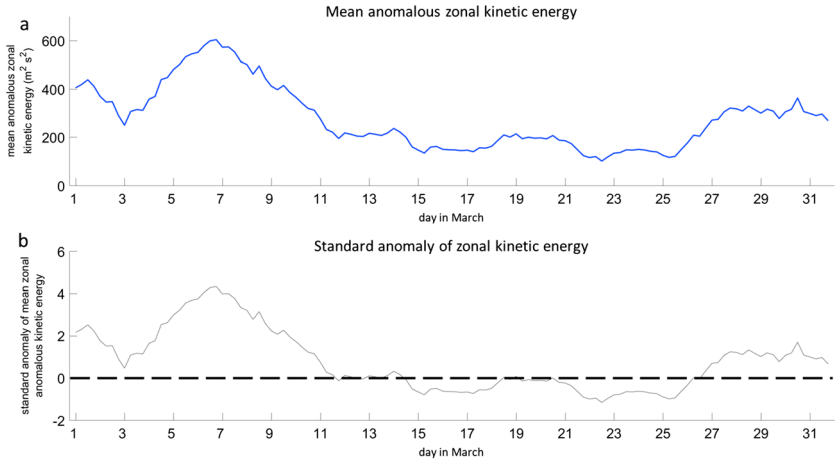

Figure 4. (a) Mean 200-hPa zonal EKE per unit mass (in m^2/s^2) from 6-hourly NCEP/NCAR reanalysis over the subtropical Pacific Ocean between 140°–120°W and 20°–40°N (see Figure 3) and (b) standardized anomalies of zonal EKE from (a), both from 01 to 31 March 2016. Dashed line in (b) indicates zero standard anomaly.

EKE for 06 March 2016 was 570 m^2/s^2, a magnitude matched in the reanalysis only 3 times in March since 1948 (Figures 5a and 5c). This type of long, highly zonal jet tends to be baroclinically unstable due to its long wavelength (Kundu et al., 2012). Indeed, at 1200 UTC 06 March 2016 (Figure 3d) the jet approached the wavelength of maximum baroclinic growth (5,500 km) identified by Holton (2004).

The result of this baroclinic instability can be seen by 1200 UTC 07 March 2016, in the development of a prominent ridge along 150°W (Figure 3e). By 1200 UTC 08 March 2016, the ridge axis extended from 20°N, 150°W to 45°N, 130°W and began to undergo anticyclonic wave breaking between 35° and 45°N (similar to that observed in Ryoo et al., 2013; Figure 3f). That wave breaking led to the development of a deep trough between 15 and 25°N. This trough was marked by strongly negative height anomalies (approaching −250 m) over northwest Mexico and the adjacent southwest United States (110°W; Figure 3f). By 1200 UTC 09 March 2016, this trough had moved southeast, over west-central Mexico, with 200-hPa height anomalies approaching −300 m at some grid points (Figure 3g). At 1200 UTC 10 March 2016, the mean 6-hr, 200-hPa height anomaly near Mexico City reached −220 m (Figures 3h and 6a), a value that was more than 4 standard deviations below normal for March (over the period 1948–2017; Figure 6b). Indeed, the daily 200-hPa height anomaly also exceeded −200 m (Figure 7a), which is the lowest daily anomaly in March in this region in the NCEP/NCAR reanalysis (Figures 7b and 7c). From 11 through 18 March 2016, the trough slowly moved eastward and filled (not shown), and zonal EKE of the Pacific jet weakened to near 100 m^2/s^2 (Figure 4a) and standard anomalies weakened to within ±0.5 (Figure 4b), indicating a return to a more normal flow pattern.

3.3. Tropopause Fold and STE (10–12 March 2016)

A time-height series of O_3 (Figures 8a and 8b) and PV (Figures 8c and 8d) in the atmospheric column over Mexico City shows the impact of this very deep trough on the middle and upper troposphere. On 03–05 March 2016, there appears to have been weak STE, with a stratospheric intrusion down to nearly 250 hPa (traced out by the 2-PVU contour extending from the stratosphere, which is a widely used marker for the dynamical tropopause; Holton et al., 1995; Figures 8c and 8d). This STE was likely associated with a weak trough (200-hPa height anomalies of −50 m; see Figures 3a and 3b) that crossed south-central Mexico the first five days of March. However, the strongest PVU anomalies in the troposphere appeared on 10 March 2016 (Figures 8c and 8d). By 11 March 2016, the 4-PVU contour extends all the way down to 300 hPa, the 2-PVU contour extends to 350 hPa, and the 0.5-PVU contour extends past 550 hPa (Figures 8c and 8d). This PV intrusion began as the strong upper level trough reached its peak intensity over central Mexico (Figure 3h). The STE persisted in central Mexico for approximately 48 hr, marked by high values of PVU below 200 hPa (Figures 8c and 8d). It is clear from the multiple continuous PV contours (2 PVU in both ERA-Interim and MERRA-2, and 4 PVU in MERRA-2) connecting the troposphere with the stratosphere,

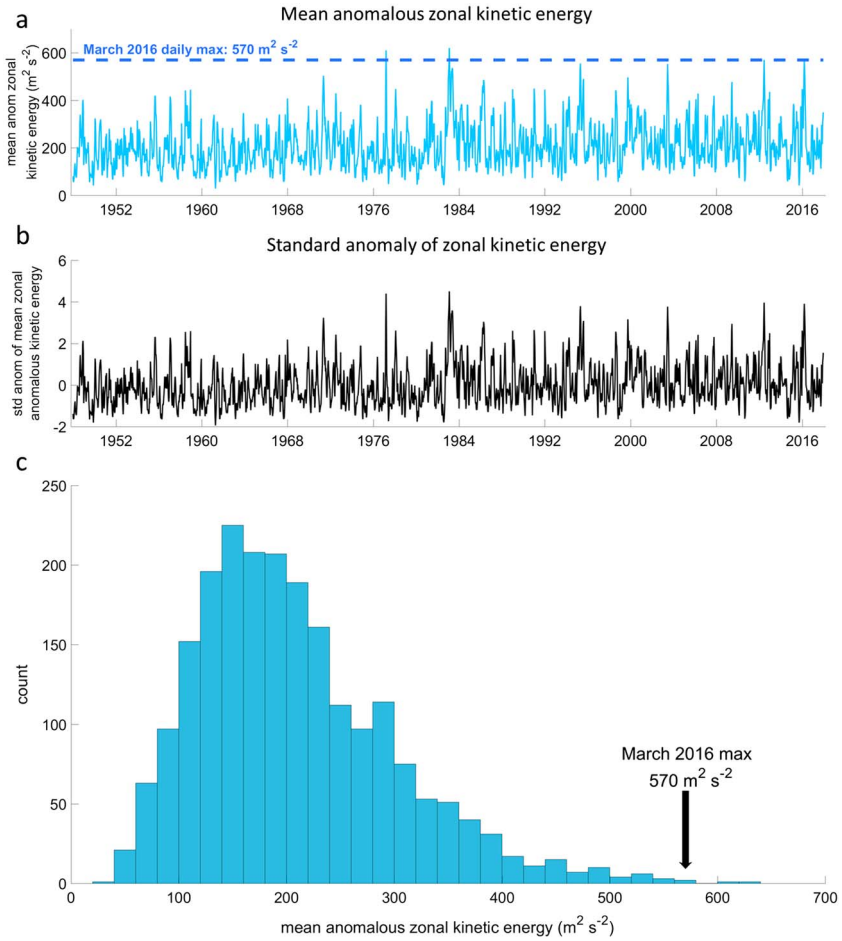

Figure 5. (a) Mean 200-hPa zonal EKE per unit mass (in m^2/s^2) from daily NCEP/NCAR reanalysis over the subtropical Pacific Ocean between 140°–120°W and 20°–40°N (see Figure 3), (b) standardized anomalies of the EKE in (a), and (c) histogram of mean zonal EKE in (a). All panels show all March days, 1948–2017. Arrow in (c) indicates maximum value observed in March 2016.

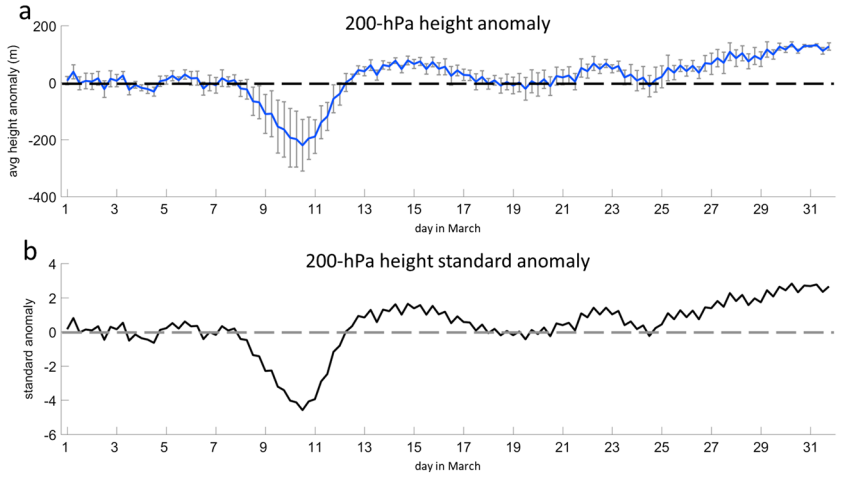

Figure 6. (a) Mean (blue curve) and standard deviation (bars) 200-hPa height anomalies (in m) from 6-hourly NCEP/NCAR reanalysis over central Mexico between 105°–95°W and 17.5°–22.5°N (see Figure 3) and (b) standardized anomalies of heights in (a), both for 01–31 March 2016. Dashed lines in (a) and (b) indicate zero anomaly.

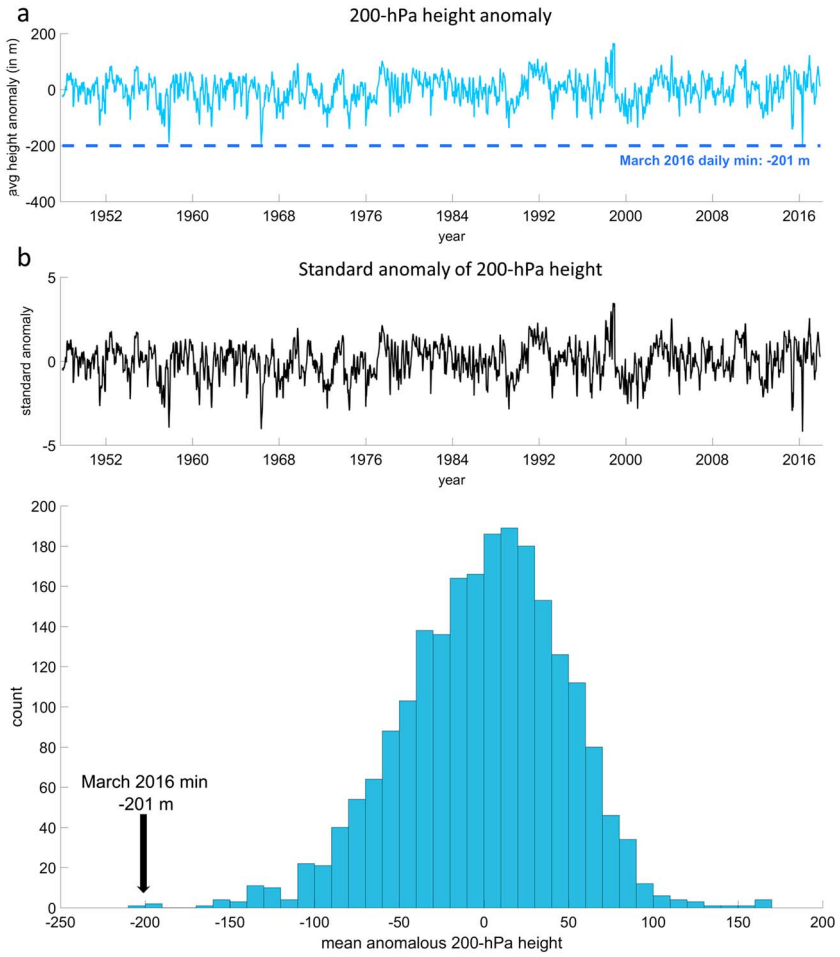

Figure 7. (a) Mean 200-hPa height anomalies (in m) from daily NCEP/NCAR reanalysis over central Mexico between 105°–95°W and 17.5°–22.5°N (see Figure 3), (b) standardized anomalies of the heights in (a), and (c) histogram of mean heights in (a). All panels show all March days, 1948–2017. Arrow in (c) denotes minimum value observed in March 2016.

that significant amounts of stratospheric air were entrained well into the troposphere as a result of the passage of the upper level trough. By 13 March 2016, high-PVU air no longer extended deep into the troposphere over Mexico City.

Further strong evidence of STE can be seen in the time-height series of O_3 concentration centered on Mexico City (Figures 8a and 8b). Throughout March 2016, the O_3-rich lower stratosphere, with concentrations from 400 to over 1,200 ppb, is bounded at about 100 hPa by the tropopause. Beginning on 10 March 2016 and continuing through 12 March 2016, O_3 concentrations exceeding 200 ppb are present throughout the upper troposphere, and values exceeding 75 ppb extend nearly to the surface. These high O_3 concentrations were located deep into the troposphere in the two independent reanalyses (MERRA-2 (Figure 8c) and ERA-Interim (Figure 8d)), thus offering additional strong evidence of the STE. These stratospheric-origin O_3 molecules were likely entrained into the deeply mixed boundary layer of 11 March 2016, evidenced by the dry adiabatic lapse rates extending from the surface to 530 hPa on the 0000 UTC 12 March 2016 sounding from Mexico City (Figure 9a).

These high O_3 concentrations in the lower and middle troposphere, when combined with a deeply mixed boundary layer on 11 March 2016, likely contributed to the onset of the high O_3 event on 12 March 2016. Furthermore, some of the O_3 likely remained in the residual nocturnal ABL (e.g., Couach et al., 2003; Pérez-Vidal & Raga, 1998; Raga et al., 1999), and mixed down to the surface in subsequent days. However, by 0000 UTC 13 March 2016, most of the stratospheric O_3 was no longer directly over Mexico

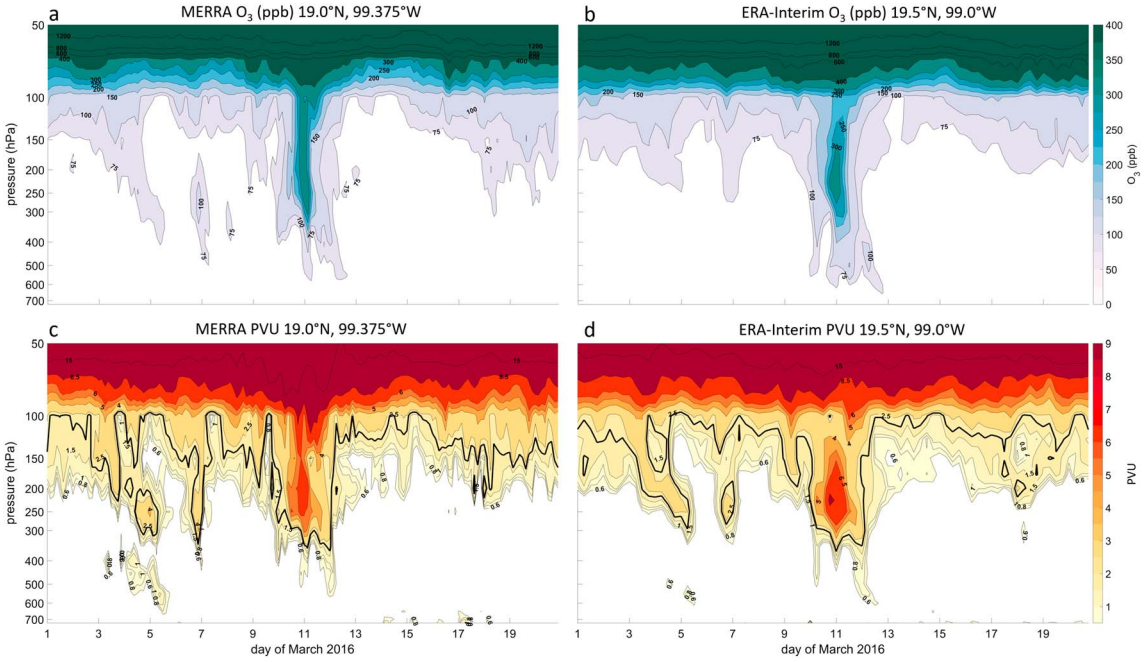

Figure 8. Time-height cross sections of O_3 concentration (in ppb) from (a) MERRA-2 and (b) ERA-Interim centered over Mexico City from 01 to 20 March 2016. (c and d) Same as (a) and (b) but for potential vorticity (in PVU). MERRA-2 values taken from the grid point at 19.0°N, 99.375°W, and ERA-Interim values taken from the grid point at 19.5°N, 99.0°W. The 2-PVU contour is bold in (c) and (d). All times in UTC.

City (Figures 8a and 8b). The extreme O_3 event at the surface peaked on 15 March 2016, nearly 72 hr after peak STE, suggesting that another physical mechanism likely also contributed to the surface O_3 event.

3.4. High Surface O_3 Event (13–16 March 2016)

Surface O_3 in Mexico City is often the result of a combination of factors: abundant O_3 precursors, strong UV radiation, generally weak horizontal winds, and poor ventilation. Between 2011, when the city government's air quality contingency plan was updated, and March 2016, ambient O_3 concentrations in Mexico City did not reach levels that would trigger (greater than 184 ppb) government-established actions to limit further emissions of O_3 precursors (SEDEMA, 2017). It is also important to note that in July 2015, the environmental authorities removed the operating restriction on private vehicles older than eight years, allowing them to operate every day of the week as long as the vehicle met certain emission limits. This action increased vehicular traffic by 20% in a six-month period and also increased the emission of O_3 precursors associated with vehicular exhaust emissions (Velasco & Retama, 2017).

Due to subsidence associated with the departure of the extreme cutoff low, the deep adiabatic boundary layer observed on 12 March (Figure 9a) was followed on subsequent days by the development of a strong capping inversion and the presence of very weak winds in the lower troposphere (Figures 9 and 10). On 13, 14, and 15 March 2016, a 2–3 °C thermal inversion near 600–650 hPa was sampled by the 1200 UTC radiosondes (Figures 9b–9d). This inversion was located only about 1,500–2,000 m above ground level, and given that maximum 2-m air temperatures only reached between 25 and 28 °C (not shown), the inversion acted to limit the growth of the ABL to no more than about 2,000 m above ground level. This ABL depth is about 1,000 m smaller than the March climatology reported by García-Franco et al. (2018). The thermal inversion also prevented the development of deep convective clouds and precipitation, allowing strong UV-B radiation to continue through the afternoon hours. Indeed, from 9 to 16 March 2016, the average daily UV-B radiation measured at Merced station (2,160 m above ground level) approached or exceeded 2 MED/hr (Figure 11a); for Merced, UV-B values over 2 MED/hr are rare for any month of the year (Figure 11b) and indicate strong UV radiation. Nearby stations (SAG and TLA) recorded average daily UV-B of more than 1.75 MED/hr. Finally, as the upper level trough departed to the east, neutral heights and a weak flow regime developed, with wind speeds less than 3 m/s observed from the surface (770 hPa) to the inversion (650–

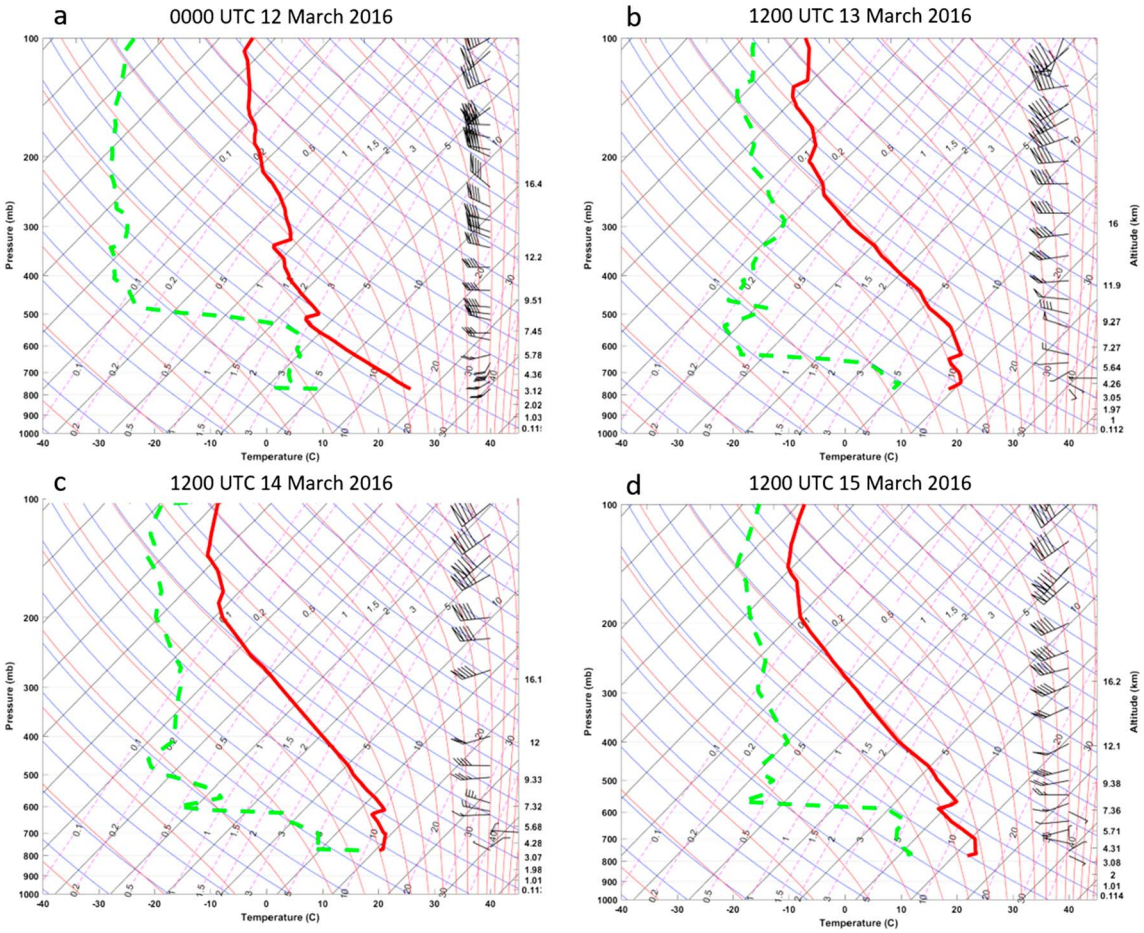

Figure 9. Radiosonde upper air observations (temperature and dew point temperature in °C, wind in kt) from Mexico City (Tacubaya station 76679) from (a) 0000 12 March 2016 (1900 local time) and (b–d) 1200 UTC 13–15 March 2016 (0700 local time).

600 hPa) at 1200 UTC from 13 to 15 March 2016 (Figures 9b–9d and 10b), and stronger flow on each day was only confined to levels above the thermal inversion. Inside the ABL on 13–15 March 2016, horizontal winds above Mexico City returned to the typical (and highly variable) mesoscale circulations (de Foy et al., 2006; Figure 10a), which likely aided in recirculating O_3 and precursor species from the previous day back into the boundary layer the next day (Pérez-Vidal & Raga, 1998; Velasco et al., 2008), thus promoting an increase in O_3 concentrations each day during the multiday event.

Concentrations of CO dropped on 9–10 March (Wednesday–Thursday; Figure 2b) due to strong southerly surface flow (Figure 10a) and upward vertical velocity (Figure 10c) coupled to the passage of the upper level trough (Figures 3g and 3h). This flow enhanced ventilation and the typical rush hour peaks were absent (not shown). Weak winds (less than 2 m/s) on the early morning of Friday 11 March drove a CO increase during the following morning rush hour (not shown), but strong winds between 0800 and 1900 (local time) dispersed the pollutants rapidly. With the departure of the trough, CO concentration increased, and the typical diurnal CO variability returned with a clear peak in the morning and somewhat lower peak in the late afternoon (not shown). Daily CO average concentrations increased progressively from Friday 11 to Monday 14 March, passing from 0.50 to 0.89 ppm (Figure 2b). High concentrations of CO on Sunday are unusual because of the significant vehicular traffic reduction. Nocturnal CO concentrations (2200–0400 local time) also increased in the same period, reaching a value of 0.89 ppm on Sunday 13 March (not shown), suggesting a recirculation of pollutants, particularly of O_3 precursors associated with vehicular emissions (Jaimes-Palomera et al., 2016).

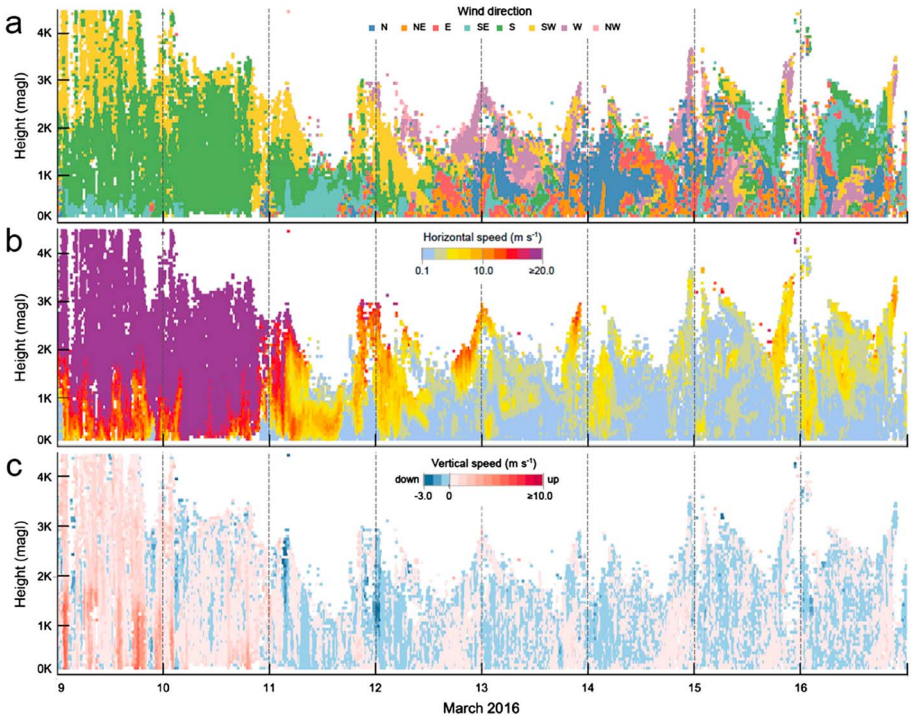

Figure 10. Vertical profile above Mexico City of (a) mean wind direction (named by where the wind comes from), (b) wind speed (in m/s), and (c) vertical wind speed (in m/s), from 09 to 16 March 2016 (time in UTC).

On Monday 14 March 2016, the atmospheric stagnation continued and favored the accumulation of O_3 and precursor species from the previous days. The presence of an intense thermal inversion limited the vertical exchange with the free troposphere, and that, in combination with strong solar radiation and the incorporation of fresh NO_x emissions, likely enhanced the O_3 production. Several monitoring stations recorded O_3 concentrations greater than 180 ppb, with an hourly maximum of 210 ppb in the early afternoon at CUA station. In response the authorities activated the level 1 measures of the contingency plan ("Fase I de Contingencia Ambiental").

Unfortunately, some of those mitigation actions may have worsened the O_3 problem. For example, the government-imposed limits on motor vehicle circulation (which reduced circulation by about 20% on Tuesday 15 March 2016 from 0500 to 2200 local time) and operation of some major industries may have led to reductions in the emission of O_3 precursors, but not necessarily in O_3 ambient concentration. According to the local emission inventory (SEDEMA, 2018), 85% and 17% of NO_x and VOC emissions, respectively, have their origin in vehicular traffic, while 4% and 8% of NO_x and VOC emissions come from point sources (such as industries). A significant reduction of NO_x emissions in a VOC-sensitive regime could have influenced the O_3 formation, similar to the effect described by Stephens et al. (2008). Small incremental reductions in NO_x emissions have proved in other studies to be ineffective, and possibly detrimental, by enhancing the O_3 production (Lei et al., 2008; Song et al., 2010). The additional vehicular restrictions in this case seemed to be largely ineffective, since the O_3 levels were still high on Tuesday 15 March 2016. In response, the authorities implemented even stricter vehicular restrictions on the next day (in effect Wednesday 16 March 2016).

The air quality annual report for 2016 prepared by the government (SEDEMA, 2017) provides further evidence of some of the unusual meteorological aspects of this event, in particular vertical profiles of the horizontal wind. The change from high surface wind conditions associated with the deep upper tropospheric trough to weak surface winds after the trough moved eastward is clearly seen in the 60-min observations (Figure 10), further supporting the evidence of poor ventilation as seen in the once-daily radiosondes (Figure 9). In summary, it is clear that several ingredients—meteorological, photochemical, and

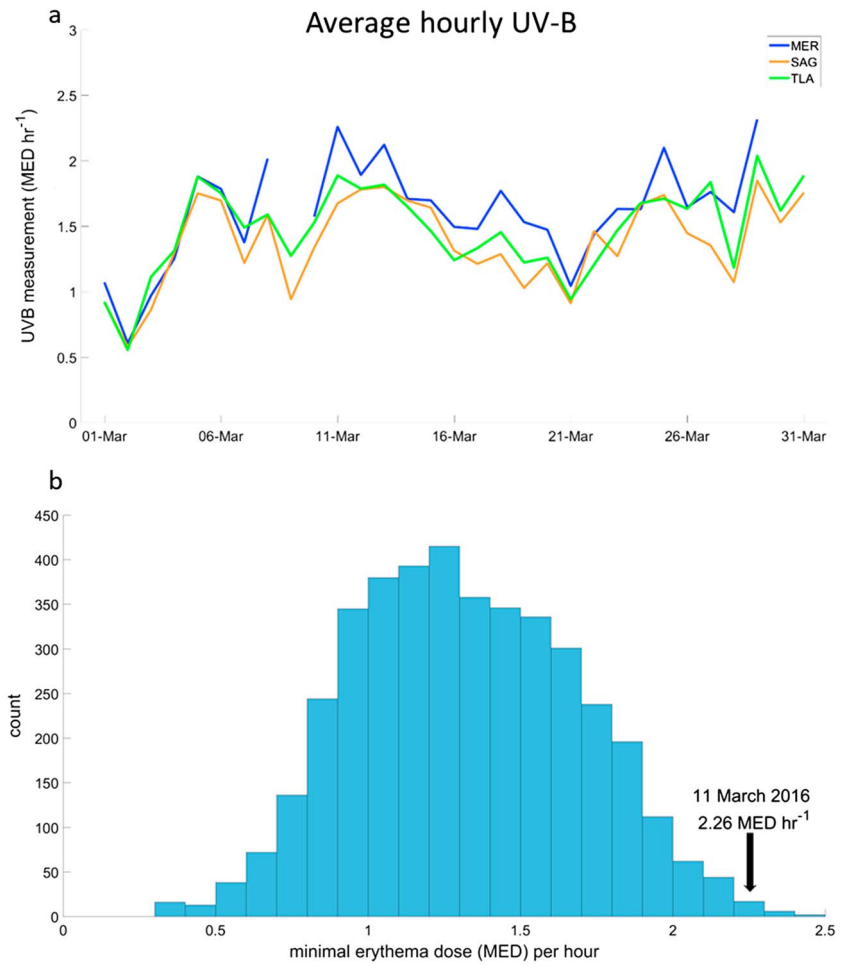

Figure 11. (a) Average daily UV-B measurements (in MED/hr) for stations in the RAMA observing network in Mexico City for 01–31 March 2016 and (b) histogram of daily UV-B concentrations at station Merced (MED; blue curve in (a)) for all March months 2004–2017. Highest UV-B measurement on 11 March 2016 indicated by black arrow.

government actions—combined to extend the stratospheric O_3 intrusion event (on 10–12 March 2016) into a hazardous, multiday local surface O_3 event (from 13 to 17 March 2016) in Mexico City.

4. Conclusions and Discussion

This study analyzed the physical mechanisms behind the unusual and hazardous surface O_3 event of March 2016 in Mexico City. From 03 to 07 March 2016, zonal EKE increased to highly unusual levels as a very strong, zonally oriented jet extended across much of the subtropical Pacific. That zonal jet quickly evolved into waves due to its baroclinic instability, and Rossby wave breaking of a pronounced ridge along 150°W led to the development of a very deep cutoff upper level low. The cutoff low crossed central Mexico with 200-hPa heights at levels not seen in the 70-year reanalysis record. Meanwhile, strong downward motions on the western side of the cutoff low led to significant STE, with 2-PVU air extending down to nearly 400 hPa in the air column above Mexico City (a level only about 5,000 m above ground level). That STE event transported O_3-rich stratospheric air well into the troposphere, with concentrations of 100 ppb in ERA-Interim reanalysis (75 ppb in MERRA-2 reanalysis) down to nearly 600 hPa. However, the strong surface O_3 event was not limited to 12 March 2016, when a deep ABL very likely transported some of that stratospheric O_3 to the surface. Indeed, the highest surface O_3 concentrations were measured on 15 March 2016, nearly 48 hr after the STE event and the pronounced intrusion of stratospheric O_3 into the troposphere.

To explain this multiday O_3 event, the following physical pathway is proposed.

1. First, the subtropical Pacific jet strengthened and lengthened. The zonal jet extension occurred possibly due to the mechanism proposed by Weickmann and Berry (2007, 2009): a very active Madden-Julian Oscillation event traversed the Maritime Continent and Western Pacific in February 2016 (leading to a strengthening of the subtropical jet in early March), which then transitioned into the Western Hemisphere and Indian Ocean the first week of March 2016 (leading to an increase in jet waviness after 07 March 2016). This physical mechanism is supported by Barrett and Raga (2016), who noted that high surface O_3 concentrations in Mexico City tend to be favored on days when the Real-time Multivariate Madden-Julian Oscillation (Wheeler & Hendon, 2004) index is in phases 2 and 3, which it was from 09 to 13 March 2016.
2. Second, the subtropical jet became baroclinically unstable and wavy.
3. Third, one of those waves, a pronounced anticyclonic ridge along 150°W, underwent anticyclonic wave breaking between 35 and 45°N.
4. Fourth, that wave breaking led to the development of an anomalously deep and equatorward cutoff low between 15 and 25°N.
5. Fifth, the deep low brought O_3-rich stratospheric air well into the troposphere via a pronounced STE event seen in vertical profiles of both PV and O_3 concentration in the air column above Mexico City. This O_3-rich air remained in the air column on 11 and 12 March 2016, likely mixing to the surface on those days and re-entraining into the ABL due to basin-wide mesoscale circulations on 13 March 2016.
6. Sixth, subsidence behind the low both suppressed the development of convective clouds and led to the formation of strong thermal inversions near 650 hPa. Both of those factors contributed to strong UV-B radiation reaching the surface from 13 to 15 March 2016.
7. Seventh, and finally, weak height gradients behind the departing low led to poor ventilation of the Mexico City metropolitan region, with stronger synoptic-scale flow confined to the region above the thermal inversions.

Combined with these meteorological conditions, government actions may have also contributed to the persistent high O_3 ambient concentrations between 13 and 16 March. For example, the well-known springtime "weekend effect" in Mexico City occurred on Sunday 13 March, whereby even though fewer vehicles were in circulation (because it was a Sunday), O_3 concentrations were not necessarily reduced. The vehicular restrictions implemented as a mitigation action by authorities on Monday afternoon 14 March may have contributed to extend this effect, reducing O_3 destruction during the night, therefore allowing O_3 concentrations to reach even higher levels on 15 March, as a consequence of starting from higher-than usual early-morning levels.

The results of this study highlight the need to consider meteorological factors when analyzing events with high surface O_3 concentrations. This study also shows the importance of both stratospheric and tropospheric processes to the generation of surface O_3 in Mexico City. Government policymakers are encouraged to consider both potential STE events and upper troposphere features that portend subsidence, poor ventilation, and the development of thermal inversions, as all of these may lead to hazardous surface O_3 concentrations in the metropolitan area. The large waviness experienced by the jet stream and the cutoff low and STE event associated with the beginning of the high surface O_3 event in March 2016 was extremely unusual, not seen before in the available reanalysis data set that dates back 70 years to 1948. Many studies have warned that extreme events in various meteorological parameters are projected to become more frequent in the changing climate. However, few studies have explored the frequency of cutoff lows and STE events at the latitude of Mexico City. More research is needed to determine their potential role in high surface O_3 events at tropical latitudes in the future. This study provides additional evidence on the complexity of the air quality management in the Mexico City megalopolis. The possible influence of synoptic meteorology is usually not considered during the design or evaluation of the environmental management plans. In light of our results, the use of modeling studies to evaluate the relative role of stratospheric ozone and the synoptic-scale phenomena on local air quality is necessary. Similarly, modeling studies would be a useful tool to evaluate in advance the impacts that some mitigation actions being considered for implementation could have on the air quality of the megalopolis.

Acknowledgments

This work was partially supported by the Programa de Estancias de Investigación, Dirección General de Personal Académico, Universidad Nacional Autónoma de México (DGAPA-UNAM). The air quality data were obtained from the databases of the Mexico City's Air Quality Monitoring Network (http://www.aire.cdmx.gob.mx/default.php), operated by the Ministry of Environment of Mexico City. Radar wind profiler data are available by request from the Mexico City's Air Quality Monitoring Network. ERA-Interim reanalysis data were downloaded from ECMWF (http://apps.ecmwf.int/datasets/) and MERRA-2 reanalysis data were downloaded from NASA (NASA GES DISC online archive https://disc.gsfc.nasa.gov/uui/datasets). Radiosonde observations were obtained from the University of Wyoming online archive (http://weather.uwyo.edu/upperair/sounding.html). A. Retama thanks E. Velasco for his insightful comments. Finally, the authors declare they have no competing interests.

References

Akritidis, D., Pozzer, A., Zanis, P., Tyrlis, E., Škerlak, B., Sprenger, M., & Lelieveld, J. (2016). On the role of tropopause folds in summertime tropospheric ozone over the eastern Mediterranean and the Middle East. *Atmospheric Chemistry and Physics*, *16*(21), 14,025–14,039. https://doi.org/10.5194/acp-16-14025-2016

Anenberg, S. C., West, I. J., Fiore, A. M., Jaffe, D. A., Prather, M. J., Bergmann, D., et al. (2009). Intercontinental impacts of ozone pollution on human mortality. *Environmental Science and Technology*, *43*(17), 6482–6487. https://doi.org/10.1021/es900518z

Barrett, B. S., & Raga, G. B. (2016). Variability of winter and summer surface ozone in Mexico City on the intraseasonal timescale. *Atmospheric Chemistry and Physics*, *16*(23), 15,359–15,370. https://doi.org/10.5194/acp-16-15359-2016

Büker, M. L., Hitchman, M. H., Tripoli, G. J., Pierce, R. B., Browell, E. V., & Avery, M. A. (2005). Resolution dependence of cross-tropopause ozone transport over East Asia. *Journal of Geophysical Research*, *110*, D03107. https://doi.org/10.1029/2004JD004739

Cooper, O. R., Foster, C., Parrish, D., Trainer, M., Dunlea, E., Ryerson, T., et al. (2004). A case study of trans-Pacific warm conveyor belt transport: The influence of merging airstreams on trace gas import to North America. *Journal of Geophysical Research*, *108*, D23S08. https://doi.org/10.1029/2003JD003624

Cooper, O. R., Parrish, D. D., Stohl, A., Trainer, M., Nédélec, P., Thouret, V., et al. (2010). Increasing springtime ozone mixing ratios in the free troposphere over western North America. *Nature*, *463*(7279), 344–348. https://doi.org/10.1038/nature08708

Couach, O., Balin, I., Jiménez, R., Ristori, P., Perego, S., Kirchner, F., et al. (2003). An investigation of ozone and planetary boundary layer dynamics over the complex topography of Grenoble combining measurements and modeling. *Atmospheric Chemistry and Physics*, *3*(3), 549–562. https://doi.org/10.5194/acp-3-549-2003

Crutzen, P. (1973). Discussion of chemistry of some minor constituents in stratosphere and troposphere. *Pure Applied Geophysics*, *106*, 1385–1399.

Danielsen, E. F. (1968). Stratosphere-tropospheric exchange based upon radioactivity, ozone, and potential vorticity. *Journal of the Atmoshperic Sciences*, *25*, 502–518.

Dee, D. P., Uppala, S. M., Simmons, A. J., Berrisford, P., Poli, P., Kobayashi, S., et al. (2011). The ERA-Interim reanalysis: Configuration and performance of the data assimilation system. *Quarterly Journal of the Royal Meteorological Society*, *137*(656), 553–597. https://doi.org/10.1002/qj.828

Dempsey, F. (2014). Observations of stratospheric O_3 intrusions in air quality monitoring data in Ontario, Canada. *Atmospheric Environment*, *98*, 111–122. https://doi.org/10.1016/j.atmosenv.2014.08.024

de Foy, B., Varela, J. R., Molina, L. T., & Molina, M. J. (2006). Rapid ventilation of the Mexico City basin and regional fate of the urban plume. *Atmospheric Chemistry and Physics*, *6*(8), 2321–2335. https://doi.org/10.5194/acp-6-2321-2006

Doran, J. C., Abbott, S., Archuleta, J., Bian, X., Chow, J., Coulter, R. L., et al. (1998). The IMADA-AVER boundary layer experiment in the Mexico City area. *Bulletin of the American Meteorological Society*, *79*(11), 2497–2508. https://doi.org/10.1175/1520-0477(1998)079<2497:TIABLE>2.0.CO;2

Dragani, R. (2011). On the quality of the ERA-Interim ozone reanalyses: Comparisons with satellite data. *Quarterly Journal of the Royal Meteorological Society*, *137*(658), 1312–1326. https://doi.org/10.1002/qj.82110.1002/qj.821

Edgerton, S. A., Bian, X., Doran, J. C., Fast, J. D., Hubbe, J. M., Malone, E. L., et al. (1999). Particulate air pollution in Mexico City: A collaborative research project. *Journal of the Air and Waste Management Association*, *49*(10), 1221–1229. https://doi.org/10.1080/10473289.1999.10463915

EPA (2006). Peak air quality statistics for the six principal pollutants by metropolitan statistical area, Environmental Protection Agency, Washington, D.C., 2003.

Fast, J. D., & Zhong, S. (1998). Meteorological factors associated with inhomogeneous ozone concentrations within the Mexico City basin. *Journal of Geophysical Research*, *103*(D15), 18,927–18,946. https://doi.org/10.1029/98JD01725

García-Franco, J. L., Stremme, W., Bezanilla, A., Ruiz-Angulo, A., & Grutter, M. (2018). Variability of the mixed-layer height over Mexico City. *Boundary-Layer Meteorology*, *167*(3), 493–507. https://doi.org/10.1007/s10546-018-0334-x

García-Yee, J. S., Torres-Jardón, R., Barrera-Huertas, H., Castro, T., Peralta, O., García, M., et al. (2018). Characterization of NO_x -O_x relationships during daytime interchange of air masses over a mountain pass in the Mexico City megalopolis. *Atmospheric Environment*, *177*, 100–110. https://doi.org/10.1016/j.atmosenv.2017.11.017

Gelaro, R., McCarty, W., Suárez, M. J., Todling, R., Molod, A., Takacs, L., et al. (2017). The Modern-Era Retrospective Analysis for Research and Applications, version 2 (MERRA-2). *Journal of Climate*, *30*(14), 5419–5454. https://doi.org/10.1175/JCLI-D-16-0758.1

GMAO (2015). MERRA-2 inst3_3d_asm_Np: 3d, 3-hourly, instantaneous, pressure-level, assimilation, Assimilated Meteorological Fields v5.12.4, Goddard Space Flight Center Distributed Active Archive Center (GSFC DAAC). Greenbelt, MD. https://doi.org/10.5067/QBZ6MG944HW0

Holton, J. R. (2004). *An Introduction to Dynamic Meteorology* (4th ed., Vol. 88, p. 547). Waltham, USA: International Geophysics Series, Academic Press.

Holton, J. R., Haynes, P. H., McIntyre, M. E., Douglass, A. R., Rood, R. B., & Pfister, L. (1995). Stratosphere-troposphere exchange. *Reviews of Geophysics*, *33*(4), 403–440. https://doi.org/10.1029/95RG02097

Jacob, D. J. (1999). *Introduction to Atmospheric Chemistry*. Princeton, USA: Princeton University Press.

Jaimes-Palomera, M., Retama, A., Elias-Castro, G., Neria-Hernández, A., Rivera-Hernández, O., & Velasco, E. (2016). Non-methane hydrocarbons in theatmosphere of Mexico City: Results of the 2012 ozone-season campaign. *Atmospheric Environment*, *31*, 260–263. https://doi.org/10.1016/j.scs.2016.12.015

Kalnay, E., Kanamitsu, M., Kistler, R., Collins, W., Deaven, D., Gandin, L., et al. (1996). The NCEP/NCAR 40-yearreanalysis project. *Bulletin of the American Meteorological Society*, *77*(3), 437–471. https://doi.org/10.1175/1520-0477(1996)077<0437:TNYRP>2.0.CO;2

Kentarchos, A. S., & Davies, T. D. (1998). A climatology of cut-off lows at 200 hPa in the Northern Hemisphere, 1990–1994. *International Journal of Climatology*, *18*(4), 379–390. https://doi.org/10.1002/(SICI)1097-0088(19980330)18:4<379::AID-JOC257>3.0.CO;2-F

Knowland, K. E., Ott, L. E., Duncan, B. N., & Wargan, K. (2017). Stratospheric intrusion-influenced ozone air quality exceedances investigated in the NASA MERRA-2 reanalysis. *Geophysical Research Letters*, *44*, 10,691–10,701. https://doi.org/10.1002/2017GL074532

Kundu, P. K., Cohen, I. M., & Dowling, D. R. (2012). *Fluid Mechanics* (5th ed.p. 891). Amsterdam: Elsevier.

Langford, A. O., Aikin, K. C., Eubank, C. S., & Williams, E. J. (2009). Stratospheric contribution to high surface ozone in Colorado during springtime. *Geophysical Research Letters*, *36*, L12801. https://doi.org/10.1029/2009GL038367

Langford, A. O., Alvarex, R. J. II, Briooude, J., Fine, R., Gustin, M. S., Lin, M. Y., et al. (2017). Entrainment of stratospheric air and Asian pollution by the convective boundary layer in the southwestern U.S. *Journal of Geophysical Research: Atmospheres*, *122*, 1312–1337. https://doi.org/10.1002/2016JD025987

Langford, A. O., Brioude, J., Cooper, O. R., Senff, C. J., Alvarez, R. J., Hardesty, R. M., et al. (2012). Stratospheric influence on surface ozone in the Los Angeles area during late spring and early summer of 2010. *Journal of Geophysical Research*, *117*, D00V06. https://doi.org/10.1029/2011JD016766

Langford, A. O., Senff, C. J., Alvarez, R. J. II, Brioude, J., Cooper, O. R., Holloway, J. S., et al. (2015). An overview of the 2013 Las Vegas Ozone Study (LVOS): Impact of stratospheric intrusions and long-range transport on surface air quality. *Atmospheric Environment*, *109*, 305–322. https://doi.org/10.1016/j.atmosenv.2014.08.040

Lei, W., Zavala, M., de Foy, B., Volkamer, R., & Molina, L. T. (2008). Characterizing ozone production and response under different meteorological conditions in Mexico City. *Atmospheric Chemistry and Physics*, *8*(24), 7571–7581. https://doi.org/10.5194/acp-8-7571-2008

Levy, H. (1972). Photochemistry of the lower troposphere, Planet. *Space Sciences*, *20*(6), 919–935. https://doi.org/10.1016/0032-0633(72)90177-8

Levy, J. I., Chemerynski, S. M., & Sarnat, J. A. (2005). Ozone exposure and mortality—An empiric Bayes metaregression analysis. *Epidemiology*, *16*(4), 458–468. https://doi.org/10.1097/01.ede.0000165820.08301.b3

Lin, M. Y., Fiore, A. M., Cooper, O. R., Horowitz, L. W., Langford, A. O., Levy, H., et al. (2012). Springtime high surface ozone events over the western United States: Quantifying the role of stratospheric intrusions. *Journal of Geophysical Research*, *117*, D00V22. https://doi.org/10.1029/2012JD018151

Mena-Carrasco, M., Carmichael, G. R., Campbell, J. E., Zimmerman, D., Tang, Y., Adhikary, B., et al. (2009). Assessing the regional impacts of Mexico City emissions on air quality and chemistry. *Atmospheric Chemistry and Physics*, *9*(11), 3731–3743. https://doi.org/10.5194/acp-9-3731-2009

Molina, L. T., Kolb, C. E., de Foy, B., Lamb, B. K., Brune, W. H., Jimenez, J. L., et al. (2007). Air quality in North America's most populous city—overview of the MCMA-2003 campaign. *Atmospheric Chemistry and Physics*, *7*(10), 2447–2473. https://doi.org/10.5194/acp-7-2447-2007

Molina, L. T., Madronich, S., Gaffney, J. S., Apel, E., de Foy, B., Fast, J., et al. (2010). An overview of the MILAGRO 2006 campaign: Mexico City emissions and their transport and transformation. *Atmospheric Chemistry and Physics*, *10*(18), 8697–8760. https://doi.org/10.5194/acp-10-8697-2010

Monks, P. S., Archibald, A. T., Colette, A., Cooper, O., Coyle, M., Derwent, R., et al. (2015). Tropospheric ozone and its precursors from the urban to the global scale from air quality to short-lived climate forcer. *Atmospheric Chemistry and Physics*, *15*(15), 8889–8973. https://doi.org/10.5194/acp-15-8889-2015

Nieto, R., Gimeno, L., de la Torre, L., Ribera, P., Gallego, D., García-Herrera, R., et al. (2005). Climatological features of cutoff low systems in the Northern Hemisphere. *Journal of Climate*, *18*(16), 3085–3103. https://doi.org/10.1175/JCLI3386.1

Ott, L. E., Duncan, B. N., Thompson, A. M., Diskin, G., Fasnacht, Z., Langford, A. O., et al. (2016). Frequency and impact of summertime stratospheric intrusions over Maryland during DISCOVER-AQ (2011): New evidence from NASA's GEOS-5 simulations. *Journal of Geophysical Research: Atmospheres*, *121*, 3687–3706. https://doi.org/10.1002/2015JD024052

Pérez-Vidal, H., & Raga, G. B. (1998). On vertical distribution of pollutants in Mexico City. *Atmosfera*, *11*, 95–108.

Raga, G. B., Baumgardner, D., Castro, T., Martinez-Arroyo, A., & Navarro-Gonzalez, R. (2001). Mexico City air quality: A qualitative review of gas and aerosol measurements (1960–2000). *Atmospheric Environment*, *35*(23), 4041–4058. https://doi.org/10.1016/S1352-2310(01)00157-1

Raga, G. B., Baumgardner, D., Kok, G., & Rosas, I. (1999). Some aspects of boundary layer evolution in México City. *Atmospheric Environment*, *33*(30), 5013–5021. https://doi.org/10.1016/S1352-2310(99)00191-0

Raga, G. B., & Le Moyne, L. (1996). On the nature of air pollution dynamics in Mexico City—I. Nonlinear analysis. *Atmospheric Environment*, *30*(23), 3987–3993. https://doi.org/10.1016/1352-2310(96)00122-7

Reiter, E. R. (1975). Stratospheric-tropospheric exchange processes. *Reviews of Geophysics*, *13*(4), 459–474. https://doi.org/10.1029/RG013i004p00459

Rieck, J. K., Böning, C. W., Greatbatch, R. J., & Scheinert, M. (2015). Seasonal variability of eddy kinetic energy in a global high-resolution ocean model. *Geophysical Research Letters*, *42*, 9379–9386. https://doi.org/10.1002/2015GL066152

Riojas-Rodríguez, H., Alamo-Hernández, U., Texcalac-Sangrador, J. L., & Romieu, I. (2014). Health impact assessment of decreases in PM_{10} and ozone concentrations in the Mexico City metropolitan area: A basis for a new air quality management program. *Salud Pública Mexico*, *56*(6), 579–591. https://doi.org/10.21149/spm.v56i6.7384

Rodríguez, S., Huerta, G., & Reyes, H. (2016). A study of trends for Mexico City ozone extremes: 2001–2014. *Atmosfera*, *29*(2), 107–120. https://doi.org/10.20937/ATM.2016.29.02.01

Ryoo, J., Kaspi, Y., Waugh, D. W., Kiladis, G. N., Waliser, D. E., Fetzer, E. J., & Kim, J. (2013). Impact of Rossby wave breaking on U.S. West Coast winter precipitation during ENSO events. *Journal of Climate*, *26*(17), 6360–6382. https://doi.org/10.1175/JCLI-D-12-00297.1

SEDEMA (2017). Secretaría del Medio Ambiente de la Ciudad de México. Calidad del aire en la Ciudad de México, informe 2016. Dirección General de Gestión de la Calidad del Aire, Dirección de Monitoreo Atmosférico. Ciudad de México. Retrieved from http://www.aire.cdmx.gob.mx/descargas/publicaciones/flippingbook/informe-2016-calidad-del-aire-en-la-ciudad-de-mexico/mobile/informe_anual_calidad_aire_2016.pdf. Accessed 3 September 2018, 2017.

SEDEMA (2018). Secretaría del Medio Ambiente de la Ciudad de México. Inventario de Emisiones de la Ciudad de México 2016. Dirección General de Gestión de la Calidad del Aire, Dirección de Programas de Calidad del Aire e Inventario de Emisiones. Ciudad de México. Retrieved from http://www.aire.cdmx.gob.mx/descargas/publicaciones/flippingbook/inventario-emisiones-2016/mobile/inventario-emisiones-2016.pdf. Accesed 27 January 2019, 2018.

Simpson, D., Arneth, A., Mills, G., Solberg, S., & Uddling, J. (2014). Ozone—The persistent menace: Interactions with the N cycle and climate change. *Current Opinions in Environmental Sustainability*, *9*, 9–19. https://doi.org/10.1016/j.cosust.2014.07.008

Škerlak, B., Sprenger, M., Pfahl, S., Tyrlis, E., & Wernli, H. (2015). Tropopause folds in ERA-Interm: Global climatology and relation to extreme weather events. *Journal of Geophysical Research: Atmospheres*, *120*, 4860–4877. https://doi.org/10.1002/2014JD022787

Škerlak, B., Sprenger, M., & Wernli, H. (2014). A global climatology of stratosphere-troposphere exchange using the ERA-Interim data set from 1979 to 2011. *Atmospheric Chemistry and Physics*, *14*(2), 913–937. https://doi.org/10.5194/acp-14-913-2014

Song, J., Lei, W., Bei, N., Zavala, M., de Foy, B., Volkamer, R., et al. (2010). Ozone response to emission changes: A modeling study during the MCMA-2006/MILAGRO campaign. *Atmospheric Chemistry and Physics*, *10*(8), 3827–3846. https://doi.org/10.5194/acp-10-3827-2010

Sprenger, M., Croci, M. M., & Wernli, H. (2003). Tropopause folds and cross-tropopause exchange: A global investigation based upon ECMWF analyses for the time period March 2000 to February 2001. *Journal of Geophysical Research*, *108*, D128518. https://doi.org/10.1029/2002JD002587

Staley, D. O. (1960). Evaluation of potential-vorticity changes near the tropopause and the related vertical motions, vertical advection of vorticity, and transfer of radioactive debris from stratosphere to troposphere. *Journal of Meteorology*, *17*(6), 591–620. https://doi.org/10.1175/1520-0469(1960)017<0591:EOPVCN>2.0.CO;2

Stephens, S., Madronich, S., Wu, F., Olson, J. B., Ramos, R., Retama, A., & Muñoz, R. (2008). Weekly patterns of México City's surface concentrations of CO, NO_x, PM_{10} and O_3 during 1986–2007. *Atmospheric Chemistry and Physics*, *8*(17), 5313–5325. https://doi.org/10.5194/acp-8-5313-2008

Trickl, T., Vogelmann, H., Giehl, H., Scheel, H.-E., Sprenger, M., & Stohl, A. (2014). How stratospheric are deep stratospheric intrusions? *Atmospheric Chemistry and Physics*, *14*(18), 9941–9961. https://doi.org/10.5194/acp-14-9941-2014

Velasco, E., Márquez, C., Bueno, E., Bernabé, R. M., Sánchez, A., Fentanes, O., et al. (2008). Vertical distribution of ozone and VOCs in the low boundary layer of Mexico City. *Atmospheric Chemistry and Physics*, *8*(12), 3061–3079. https://doi.org/10.5194/acp-8-3061-2008

Velasco, E., & Retama, A. (2017). Ozone's threat hits back Mexico City. *Sustainable Cities and Society*, *31*, 260–263. https://doi.org/10.1016/j.scs.2016.12.015

Volkamer, R., Sheehy, P., Molina, L. T., & Molina, M. J. (2010). Oxidative capacity of the Mexico City atmosphere—Part 1: A radical source perspective. *Atmospheric Chemistry and Physics*, *10*(14), 6969–6991. https://doi.org/10.5194/acp-10-6969-2010

Wang, W.-N., Cheng, T.-H., Gu, X.-F., Chen, H., Guo, H., Wang, Y., et al. (2017). Assessing spatial and temporal patterns of observed ground-level ozone in China. *Science Reports*, *7*(1), 3651. https://doi.org/10.1038/s41598-017-03929-w

Weickmann, K., & Berry, E. (2009). The tropical Madden–Julian Oscillation and the global wind oscillation. *Monthly Weather Review*, *137*(5), 1601–1614. https://doi.org/10.1175/2008MWR2686.1

Weickmann, K. M., & Berry, E. (2007). A synoptic-dynamic model of subseasonal atmospheric variability. *Monthly Weather Review*, *135*(2), 449–474. https://doi.org/10.1175/MWR3293.1

Wheeler, M. C., & Hendon, H. H. (2004). An all-season real-time multivariate MJO index: Development of an index for monitoring and prediction. *Monthly Weather Review*, *132*(8), 1917–1932. https://doi.org/10.1175/1520-0493(2004)132<1917:AARMMI>2.0.C

Whiteman, C. D., Zhong, S., Bian, X., Fast, J. D., & Doran, J. C. (2000). Boundary-layer evolution and regional scale diurnal circulation over the Mexico Basin and Mexico Plateau. *Journal of Geophysical Research*, *105*(D8), 10,081–10,102. https://doi.org/10.1029/2000JD900039

WHO (2006). *Air Quality Guidelines: Global Update 2005: Particulate Matter, Ozone, Nitrogen Dioxide and Sulfur Dioxide*. Geneva: World Health Organization.

Wood, E. C., Herndon, S. C., Onasch, T. B., Kroll, J. H., Canagaratna, M. R., Kolb, C. E., et al. (2009). A case study of ozone production, nitrogen oxides, and the radical budget in Mexico City. *Atmospheric Chemistry and Physics*, *9*(7), 2499–2516. https://doi.org/10.5194/acp-9-2499-2009

Yan, M. L., Liu, Z. R., Liu, X. T., Duan, H. Y., & Li, T. T. (2013). Meta-analysis of the Chinese studies of the association between ambient ozone and mortality. *Chemosphere*, *93*(6), 899–905. https://doi.org/10.1016/j.chemosphere.2013.05.040

Yang, W. S., Wang, X., Deng, Q., Fan, W. Y., & Wang, W. Y. (2014). An evidence-based appraisal of global association between air pollution and risk of stroke. *International Journal of Cardiology*, *175*(2), 307–313. https://doi.org/10.1016/j.ijcard.2014.05.044

Zelaya-Ángel, O., Tomás, S., Sánchez-Sinencio, F., Altuzar, V., Mendoza-Barrera, C., & Arriaga, J. L. (2010). Atmospheric boundary layer height calculation in Mexico City derived by applying the individual Eulerian box model. *Atmosfera*, *23*, 241–251.